Appl. Phys. A 67, 265–271 (1998)

Applied Physics A
Materials
Science & Processing
© Springer-Verlag 1998

Invited paper

Manipulation of nanoparticles using dynamic force microscopy: simulation and experiments

R. Resch, A. Bugacov, C. Baur, B.E. Koel, A. Madhukar, A.A.G. Requicha, P. Will

Laboratory for Molecular Robotics, University of Southern California, 947 West 37th Place, Los Angeles, CA 90089-0781
(Fax: +1-213/740-7512, E-mail: lmr@lipari.usc.edu)

Received: 12 May 1998/Accepted: 15 May 1998

Abstract. Dynamic force microscopy (DFM) in combination with special-purpose probe control software is used as a manipulation tool for the precise positioning of single gold nanoparticles on a mica substrate covered with a poly-L-lysine film. Experimental results are presented that show how to construct arbitrary patterns of nanoparticles. The dynamic state of the cantilever during the manipulation process is studied experimentally by analyzing the simultaneously recorded non-contact amplitude and cantilever deflection. Numerical simulations guide and supplement the experiments in order to provide a physical description of the manipulation mechanism. The results presented here show that the nanoparticles are pushed along the surface once a critical contact force between tip and gold cluster is exceeded. In addition, a method for estimating the average separation between the tip apex and the sample in DFM is described.

PACS: 07.79.Lh; 85.40.Ux; 07.05.Tp

The study of nanoparticles and small molecular clusters is an area of current interest because of the unique properties of these materials [1, 2]. Colloidal nanoparticles are especially interesting because they can be produced in various well-controlled sizes and from various materials such as metals or semiconductors [3–5]. Nanoparticle patterns have a variety of potential applications, from data storage and single-electron transistors [6, 8, 9], to nanoelectromechanical systems (NEMS) fabrication, where they may serve as templates for growth or as nanocomponents that are assembled by robotic techniques to construct complex nanostructures from the bottom up.

Building arbitrary patterns of nanoparticles requires precise positioning of individual particles. This can be achieved by using the tip of a scanning probe microscope (SPM) as a robot to manipulate the particles [7, 10, 11]. We have previously reported the controlled and precise manipulation of single Au nanoparticles by using dynamic force microscopy in combination with a special-purpose probe control software on several substrates [11, 12]. With this technique, two-dimensional patterns can be successfully formed from random arrays of deposited Au particles on a given substrate. However, the mechanisms which underlie these operations are not well understood, and the selection of manipulation parameters is largely based on previous experience and trial-and-error. This paper describes a systematic study aimed at improving our understanding of nanomanipulation using DFM. We discuss the experimental procedures and manipulation protocols, simulation studies to guide the experiments, and the experimental results.

1 Manipulation procedures

The samples were prepared by depositing 15-nm gold colloidal particles (EM.GC15; Ted Pella Inc.) from aqueous solution on freshly cleaved mica substrates that had been previously coated by a poly-L-lysine film (0.1% aqueous; Ted Pella Inc.). Subsequently, the samples were annealed in air for 3 h at 80 °C.

The experiments were carried out with an AutoProbe CP® AFM (Park Scientific Instruments) operated in non-contact (NC-AFM) and intermittent-contact (IC-AFM) mode. The instrument provides the user with three main parameters for controlling its operation in DFM: (i) the frequency f_{set} of the driving excitation of the cantilever (f_{set} is usually close to the resonant frequency of the cantilever f_{res}); (ii) the free oscillation amplitude of the cantilever A_{free} (which is controlled by the amplitude of the excitation driving the cantilever); and (iii) the desired cantilever oscillation amplitude or set-point A_{set}.

Imaging and manipulation experiments were performed in air and at room temperature using commercially available triangle-shaped silicon cantilevers (Park Scientific Instruments) with integrated conical tips. Hard cantilevers had spring constants ≈ 13.0 N/m and resonant frequencies ≈ 280 kHz, whereas the corresponding values for soft cantilevers were ≈ 3.2 N/m and ≈ 90 kHz. (These are nominal values, supplied by the vendors).

Manipulation of the Au nanoparticles was achieved by using the following protocol. First, the sample is imaged. Then, utilizing the probe control software (PCS) developed

by our group [11], the user draws an arrow with the mouse over the image, and performs a single-line scan along the arrow. The user also sets two points along the specified trajectory, such that the feedback is turned off at the first point, and re-engaged at the second point. In the experiments reported here we selected trajectories containing the center of the particle to be manipulated, turned the feedback off just before encountering the particle, and turned it back on at the desired new position of the particle. PCS also provides capabilities for simultaneously acquiring several signals during the single-line scan. We recorded the oscillation amplitude A and the dc deflection D_{dc} of the cantilever.

2 Simulation

To gain some initial insight into the manipulation phenomena we conducted numerical studies of the interactions between tip, sample, and particle. We applied continuum methods similar to those described in [15–20] to the tip/sample/particle system under conditions analogous to those encountered in our experiments. The substrate is modeled as a semi-infinite half-space and the tip and the nanoparticle as spheres of radii R_T and R_P, respectively. The cantilever dynamics is approximated by a driven, damped, harmonic oscillator with an additional term corresponding to the non-linear interaction between the tip and the sample. The cantilever is driven by a harmonic displacement of its base of the form $y(t) = A_d \sin(\omega_d t)$. The tip–sample interactions are based on simple analytic potentials consisting of attractive and repulsive terms [13, 15–20].

We restrict the motion of the cantilever to the $x - z$ plane and scan the tip along the positive x direction at constant speed v_s. The cantilever dynamics is described by the following differential equation

$$\ddot{z}(t) + \left(\frac{\omega_c}{Q_c}\right)\dot{z}(t) + \omega_c^2 z(t) + F_z^{TS}(z(t), \delta) + F_z^{TP}(x(t), z(t), \delta) = \omega_c^2 A_d \sin(\omega_d t) + \frac{\omega_c \omega_d}{Q_c} A_d \cos(\omega_d t)\,, \quad (1)$$

where $x(t) = v_s t$ and $z(t)$ are the components of the position of the center of the tip sphere, $\omega_c = 2\pi f_{res}$ is the angular resonant frequency of the cantilever and Q_c its quality factor. $F^{TS}(z(t), \delta)$ and $F^{TP}(x(t), z(t), \delta)$ are the tip–substrate and tip–particle interaction forces, respectively. When objects are not in contact with each other, the tip–substrate and tip–particle interactions are modeled by the Hamaker summation of a Lennard–Jones (6–12) potential for the interaction of a sphere with a flat surface and of two spheres, respectively [13]. Indentation of the tip into the sample is modeled by an elastic repulsive term [16, 17]. The potential depends on the distance δ between the substrate and the undeflected cantilever position, and several other parameters.

The AFM measures the amplitude of the oscillation by using a lock-in amplifier, compares it with the setpoint A_{set}, and uses the feedback circuitry to move the sample towards or away from the tip to reduce the error to zero. This is equivalent to changing the z position of the substrate, δ. To simulate the feedback operation we first compute the amplitude

$$A(t) = \sqrt{A_s^2(t) + A_c^2(t)}\,, \quad (2)$$

where

$$A_s(t) = \int_t^{t+T} dt' z(t') \sin(\omega_d t')\,,$$

$$A_c(t) = \int_t^{t+T} dt' z(t') \sin\left(\omega_d t' + \frac{\pi}{2}\right). \quad (3)$$

Then, we feed it into the equations of a proportional-integral control system and compute a new value for δ.

We solve the differential equations of motion, with initial conditions $z(t = 0) = 0$ and $\dot{z}(t = 0) = 0$, numerically by using the Verlet algorithm [14]. Initially, we place the substrate and the particle sufficiently far from the tip for the interaction forces to be negligible, and let the system evolve until it reaches the steady-state amplitude A_{free}. Then we turn the feedback on and let it adjust δ until a value δ_{set} is reached, for which the system oscillates at the desired amplitude A_{set}.

Next we turn off the feedback and keep $\delta = \delta_{set}$. After the tip goes over the particle, which is at a fixed position, we turn the feedback on again, and let the system return to its steady state. This procedure simulates the system's behavior when we attempt to push a particle but fail to move it.

Figure 1 shows the results of a simulated run. A point is plotted at the (x, z) position of the center of the tip at regular increments of time equal to 1/16th of the period of the driving oscillation. The cantilever vibrates much faster than the scanning speed, and therefore a vertical slice in the figure can be viewed as a sequence of z positions during one cycle of the vibration. The parallel horizontal lines on the left and right regions of the figure correspond to the steady state, with the feedback on and $\delta = \delta_{set}$. In the middle region, the feedback is off.

The figure shows that the amplitude of the oscillation starts decreasing as the tip approaches the particle, and even-

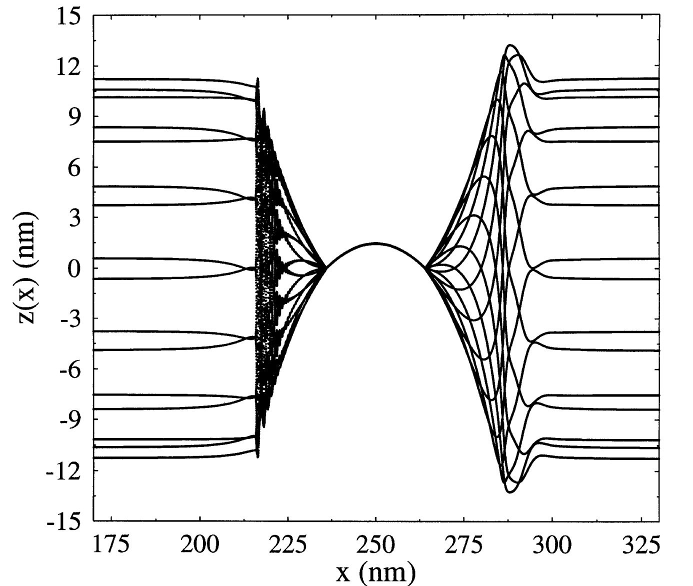

Fig. 1. Numerical simulations of the trajectory of the tip center of mass in the $x - z$ plane. The tip radius is $R_T = 45$ nm and its free equilibrium position is at $z = 0$. The particle of radius $R_P = 7.5$ nm is placed on top of the substrate and its center x-position is held fixed at $X_P = 250$ nm

tually becomes zero. The crossing patterns represent the changes in the amplitude and shifts in the phase (with respect to the driving signal) of the oscillation that are caused by the nonlinear forces between the tip and the particle as the tip approaches and leaves the interaction region.

The tip then follows the topography of the particle (convolved with the tip shape), and therefore the cantilever must deflect accordingly. As the tip leaves the interaction region, the amplitude starts to increase again and a hysteresis peak is observed before the tip loses contact with the particle [15, 21].

Figure 2 plots the cantilever oscillation amplitude A, offset by the set-point A_{set}, as a function of the x position along the scan direction. The curves 1–4 correspond to set-points in the sequence 12, 6, 3.2, and 0.8 nm, respectively. When the set-point has a large value, and therefore the tip is at a relatively large distance from the sample, the amplitude decreases while the tip passes over the particle, but remains non-zero (curve 1). As the tip approaches the particle, we observe a jump in the amplitude corresponding to the sudden transition from attractive to repulsive damping [16]. As the tip leaves the particle, we observe a small hysteresis effect before reaching the set-point value. For lower setpoints (curves 2–4), the amplitude decreases to zero during the interaction. We do not observe a jump as in curve 1 nor a hysteresis peak because the tip is already tapping on the substrate before encountering the particle.

The simulation equations have over a dozen parameters. Some of these, for example the set-point, correspond to instrument settings. But others, such as those which control the potential function, are not known or directly measurable. In the simulations we set the parameters to typical values used in the experiments, when possible, and utilize reasonable values for the others. This is consistent with our simulation goal of gaining a qualitative understanding of the manipulation process. The simulation results show that the oscillation amplitude and the cantilever deflection signals provide useful information about the systems' behavior and led us to formulate the experiments described in the next section.

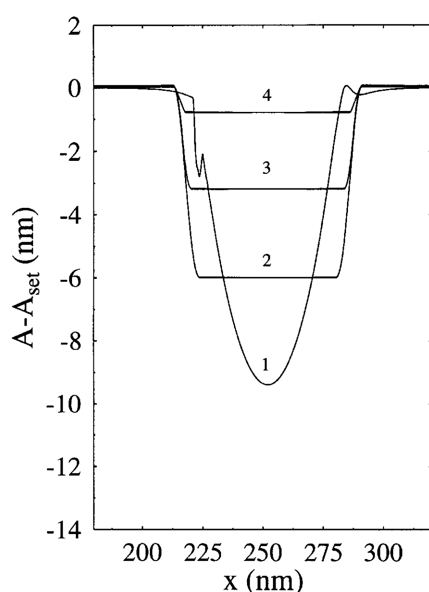

Fig. 2. Numerical simulations of the cantilever oscillation amplitude A (offset by the set-point) versus the lateral scan position x. The *curves* 1–4 correspond to set-point values equal to 12, 6, 3.2, and 0.8 nm, respectively

3 Experimental results

In the first set of experiments, we used the protocol described earlier, with $f_{set} > f_{res}$, and a hard cantilever, for each set-point in the sequence 12, 6, 3.2, and 0.8 nm. These set-points correspond to damping ratios $(1 - A_{set}/A_{free})$ ranging from 15% to 95%. The results are shown in Fig. 3. The feedback is off between the two vertical bars in the figure, and on outside the bars. The arrows on the right of Fig. 3a indicate the points where the amplitude of the tip vibration A is nearly zero, i.e., $A - A_{set} \cong -A_{set}$. A subsequent scan (not shown here) proved that the particles did not move. The following effects can be observed in Fig. 3:

– For large set-points, and hence large distances between substrate and average tip position (curves 1), the cantilever dc deflection is essentially zero, and the amplitude signal follows the topography of the nanoparticle.
– For smaller set-points (curves 2–4), the amplitude drops to zero during a portion of the scan, and the deflection increases significantly. This indicates that *the tip is in continuous contact with the particle in the region where* $A = 0$. (We also modified the experiment by setting the

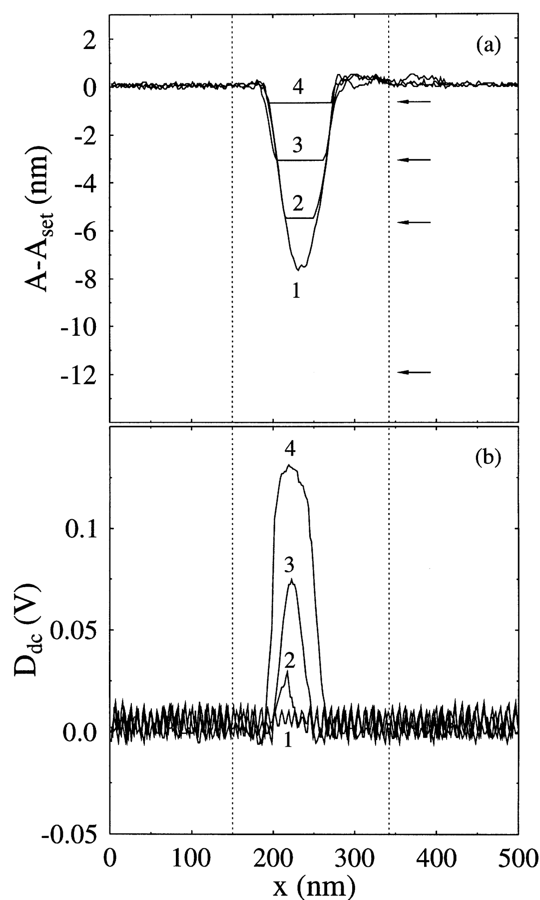

Fig. 3. a Cantilever oscillation amplitude (offset by the set-point) versus lateral scan position for set-point values equal to 12, 6, 3.2, and 0.8 nm shown as *curves* 1–4, respectively. **b** Cantilever dc deflection

driving amplitude A_{free} to zero when we switch off the feedback; we observed the same drop in amplitude, which confirms that A becomes zero in the original experiment.) The AFM images the sample in dynamic mode while the feedback is on, and then switches automatically to a constant-height contact-mode scan after the feedback is turned off. The switching point can be determined experimentally by monitoring the amplitude or the deflection (or both).

Next, we used the same protocol but recorded the maximum dc deflection of the cantilever, D_{max}, for several values of the set-point A_{set}, as shown in Fig. 4. Each curve in Fig. 4 corresponds to a different value of the driving amplitude A_{free}. Each curve was obtained by using only one cantilever, but several cantilevers, with the same nominal spring constant ≈ 13 N/m, were used in the overall experiment. Again, the particles did not move during these measurements. However, decreasing the set-points below the minimal values shown for each curve caused the particles to move. We draw the following conclusions:

- Regardless of the selected driving voltage or set-point, *the cantilever must deflect beyond a fixed threshold for the particle to move*. This threshold is $0.13\,\text{V} \pm 0.02\,\text{V}$ for the cantilevers used in the experiment. Because of the variability shown in Fig. 4, this threshold cannot be used to compute a priori the exact parameters needed to push a particle. But, rough estimates for these values are evident from the figure. Furthermore, suitable values are easy to determine experimentally for a given cantilever and driving amplitude. It suffices to step through a few set-points and monitor the maximum deflections, i.e., to trace the left portion of one of the curves in the figure until the threshold is reached.

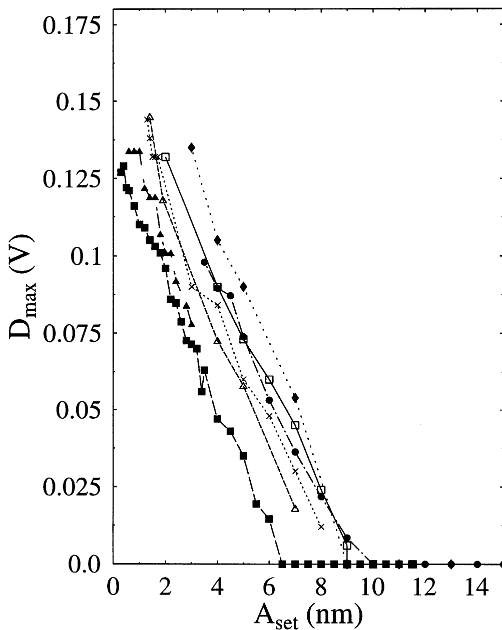

Fig. 4. Plots of the maximum cantilever dc deflection versus the set-point value, A_{set}. Each *curve* corresponds to a different value of the free oscillation amplitude ranging from 14 to 23 nm

- Because the particles do not move, the D_{max} values shown in Fig. 4 occur when the tip passes over the top of the particle. This provides useful information, as we will see below.
- Once contact with the particle is established and the cantilever starts deflecting, all of the curves show an almost linear dependence with nearly equal slopes between the set-point and maximum deflection, and this has the following consequence. In imaging mode, with the feedback on, the tip oscillates about a mean tip/substrate separation S_0, with zero dc deflection. The value of S_0, however, is unknown and not directly measurable. When the feedback is turned off, the amplitude A decays to zero, as we saw earlier, and contact is established. Then, the cantilever must deflect and climb over the particle, reaching the maximum deflection D_{max} at the top of the particle, as shown in Fig. 5. Therefore, $S_0 + D_{max} = 2R_p = H$, where H is the height of the particle, which is fixed. Since D_{max} is approximately linear with A_{set}, so is S_0. This gives an indirect (and approximate) value for the change of dc tip/sample separation that is due to a change in set-point, within the parameter range that is useful in nanomanipulation by pushing. Since $S_0 = A_{set} + S_s$, where S_s is the minimum tip/substrate separation, S_s also varies linearly with A_{set}. The *absolute* values of the dc or minimum separations remain unknown (see the discussion below).

In a third type of experiment, the same protocol was used for a range of set-points. We recorded the maximum cantilever dc deflection D_{max} shown in Fig. 6b, and the maximum amplitude drop $\Delta A = A_{set} - A_{min}$, where A_{min} denotes the minimum amplitude during the single-line scan, shown in Fig. 6a. The three curves in each of the Fig. 6a,b correspond to results obtained with a soft cantilever (▲), a hard cantilever operating at a frequency to the right of the resonance (●), and a hard cantilever operating at $f_{set} < f_{res}$ (□). The particles did not move during the measurements. For the hard cantilevers, lowering the set-points beyond those shown in the figures resulted in particle motion. This data confirms some of the results presented earlier in this paper, and provide additional information as follows:

- A pushing threshold of approximately 0.125 V for hard cantilevers is evident. It has the same value for the two curves, i.e., for operation above or below the resonant frequency.
- When a hard cantilever starts deflecting, then $\Delta A \approx A_{set}$ as shown by the straight lines with unit slope in Fig. 6a. This implies that $A_{min} = 0$, i.e., the amplitude drops to

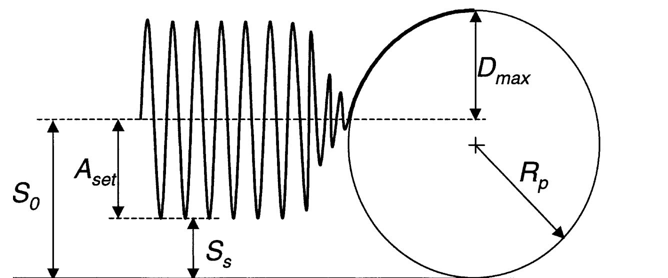

Fig. 5. Geometric relationships of the AFM tip apex and particle for set-points that cause contact with the particle

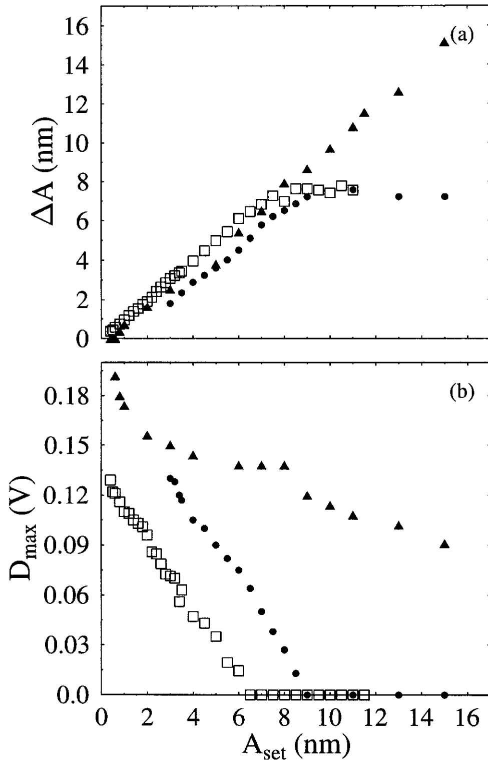

Fig. 6a,b. Drop in the cantilever amplitude signal during a scan, ΔA (**a**) and maximum cantilever deflection D_{max} (**b**) versus the setpoint value. Results are shown for a soft cantilever (≈ 3 N/m) with $f_{set} > f_{res}$ (▲) and for a hard cantilever (≈ 13 N/m) with $f_{set} < f_{res}$ (□) and $f_{set} > f_{res}$ (●)

zero and continuous contact is established, as we had seen earlier.

- For the soft cantilever, D_{max} is non-zero and $\Delta A \sim A_{set}$ for all set-points. This indicates that there is contact with the particle for all of the set-points investigated. Furthermore, the fact that the slope of the curve does not change for the whole range of set-points may be an indication that the tip was tapping on the sample. Unfortunately, during these experiments it was not possible to measure D_{max} for larger set-point values to observe any bending of this curve.
- Lowering the set-point for the soft cantilever below the values in Fig. 6 caused substrate modification but did not move the particle. Because the spring constant is approximately four times smaller for the soft than for the hard cantilever, one would expect the pushing dc deflection threshold to be four times larger (≈ 0.5 V) for the soft cantilever in order to exert the same force on the particle. But, evidently this deflection value exceeds the height of the particle and therefore the soft cantilever does not bend enough to reach this threshold; as a consequence pushing does not occur.
- At the lowest value of the set-point shown in the figures for the soft cantilever, the tip is essentially in contact with the substrate at the beginning of the scan because lowering the set-point modifies the surface (as noted above). The maximum cantilever dc deflection (0.19 ± 0.03 V) occurs approximately when the tip is over the top of the particle, and therefore corresponds to the height H of the particle. H can be measured independently by a separate scan, and is ≈ 15 nm. This provides a rough conversion factor of 80 ± 15 nm/V between the measured dc deflection signal and the actual deflection of the cantilever.
- Using a conversion factor of 80 ± 15 nm/V we estimate that the pushing threshold for the hard cantilevers is a deflection of roughly $0.125 \times 80 = 10$ nm. This corresponds to a cantilever load of about 130 nN for the manipulation of these Au nanoparticles on poly-L-lysine coated mica.
- For hard cantilevers and large set-points, the cantilever does not deflect and the amplitude drop is approximately constant. Denoting the minimum tip/substrate and tip/particle separations by S_s and S_p, respectively, the simple geometric considerations shown in Fig. 7 imply that $S_s + \Delta A - S_p = H$, or $S_s - S_p = H - \Delta A$. The measured value of ΔA is ≈ 8 nm whereas $H \approx 15$ nm. It follows that $S_s - S_p > 0$, or $S_s > S_p$, i.e., the minimum tip/sample separation is smaller over the particle (where the feedback is off) than over the substrate (where the feedback is on). Furthermore, S_s cannot be zero since S_p cannot be negative. Therefore, over the substrate *the tip is not tapping although the driving frequency is lower than the resonant frequency*. (A caveat is in order: The measured values in nm for the amplitude were obtained by using a vendor supplied, fixed calibration factor that relates the photo-detector voltage to the cantilever deflection. On-going experiments in our lab indicate that the actual calibration factor depends on the specific cantilever and experimental setup, and corresponds to lower values for the amplitudes than those reported here. These lower values do not affect the qualitative conclusions reached in this paper. The methods presented here will produce better quantitative results if the calibration factors are determined more accurately.)
- The hard cantilever curves shown in Fig. 6b or Fig. 4 provide values of D_{max} as a function of A_{set}. Because the maximum deflection occurs at the top of the particle, the geometry depicted in Fig. 5 implies that $S_0 + D_{max} = H$. Since H is known, we can estimate S_0, or alternatively the minimum separation S_s by using the conversion factor 80 nm/V derived above. For example, from the middle curve of Fig. 6b (●), we find that $A_{set} = 4$ nm corresponds to $D_{max} \approx 8.5$ nm. This implies that $S_0 \approx 6.5$ nm and the minimum separation is $S_s \approx 2.5$ nm. Therefore, with the

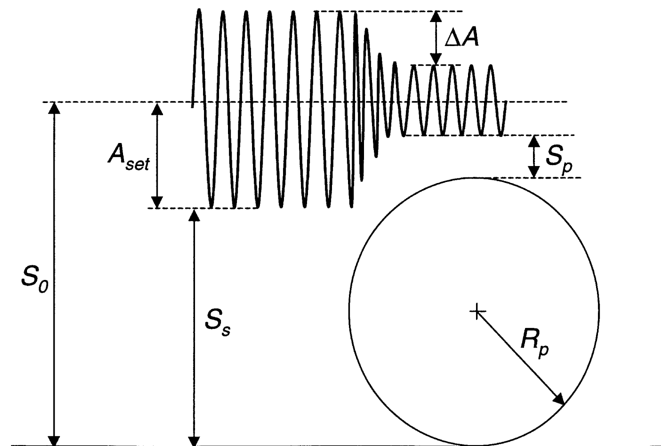

Fig. 7. Geometric relationships of the AFM tip apex and particle for set-points that do not cause continuous contact with the particle

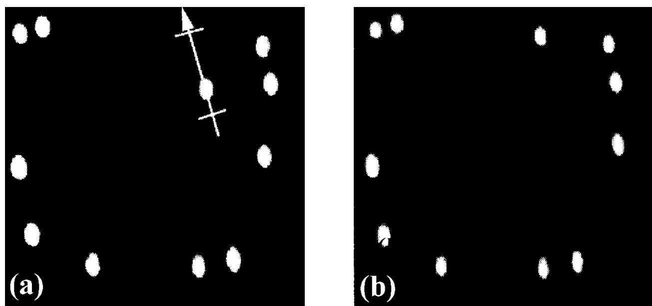

Fig. 8a,b. Pushing 15-nm Au colloids with the tip of an AFM operated in dynamic mode using PCS. **a** Scan area before pushing. The arrow indicates the particle selected for manipulation and the perpendicular bars on the arrow denote the part of the scan where the feedback is disabled. **b** Scan area after successful pushing. The manipulated particle is found in a new position relative to neighboring particles

experimental procedure described here and a calibrated deflection system (relating deflection volts to nanometers), *we can estimate the absolute values of the dc or the minimum separation between tip and sample for the AFM in dynamic mode*. The separation/set-point relationship thus derived depends only on the cantilever and substrate and is independent of the nanoparticles. The particles are needed only to measure the deflection versus set-point curves of Figs. 4 or 6b.

Figures 8 and 9 depict a successful pushing experiment. The marked particle in Fig. 8a is moved to a new position shown in Fig. 8b. Figure 9a displays the topography signal before pushing, and Fig. 9b the dc deflection during pushing. The two vertical bars denote the points where the feedback is turned off and then on again. The initial behavior is essentially the same as in the three experiments reported above for low set-points. First, the deflection increases as the tip climbs the particle. But now the pushing threshold is reached and the particle moves. The topography signal after pushing shows in Fig. 9c that part of the particle remains inside the feedback-off window, indicating that the tip does not reach the top of the particle while the feedback is disengaged. We do not know exactly what causes the small step in the deflection signal after the feedback is turned on, but we have observed that this small step often disappears when the feedback gain is adjusted.

The cantilever deflection decreases slightly after the motion begins and then remains essentially constant until the feedback is re-engaged. This decrease is akin to the difference between static and dynamic friction in macroscopic mechanics. It is consistent with our experimental observation that the pushing threshold is higher for the first time a particle is moved. This may be due to the sample preparation process. The particles may sink into the poly-L-lysine layer by a few Å during annealing, resulting in a stronger interaction with the substrate than when they rest on top of the layer after being pushed.

4 Conclusions

Single nanoparticles can be moved reliably and accurately by using dynamic force microscopy with the protocol described in this paper. We show that the manipulation pro-

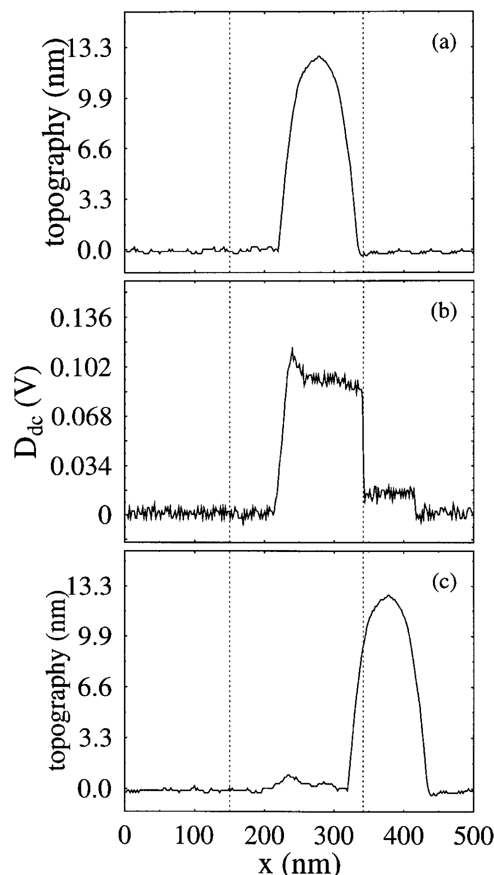

Fig. 9a–c. Experimental signals recorded during the pushing of a 15-nm Au nanoparticle with the tip of an AFM operated in dynamic mode using PCS. The feedback is disabled in the part of the scan delimited by the vertical bars. **a** Topography signal of the selected particle before pushing. **b** Deflection signal *during* pushing. **c** Topography signal after successful pushing

cess amounts essentially to pushing the particles with the tip of the instrument. The amplitude of the tip's oscillation decreases as the particle is approached, and becomes zero when uninterrupted contact is established. The tip slides up the particle until a critical value of cantilever deflection is reached, and then pushes the particle along the scan direction. This indicates that the contact force between tip and cluster is responsible for the onset of motion. Investigations with soft cantilevers (≈ 3 N/m) resulted in unsuccessful pushing. This can be explained by the soft cantilever's inability to exceed the contact force threshold necessary for pushing. Comparison between NC and IC setups (i.e., driving frequency to the right or to the left of the resonance position, respectively) shows no difference in the manipulation mechanism.

Simultaneous recording of the cantilever oscillation amplitude and dc deflection during scanning with the feedback disabled provides valuable information about the progress of a pushing operation. Furthermore, these signals can also be used to estimate the *absolute* separation between the tip and sample during normal imaging conditions in which the feedback is engaged.

Results from numerical simulations are in good qualitative agreement with the experimental data. This indicates that simple continuum methods may prove very useful in under-

standing the behavior of the AFM in dynamic mode. It may also be possible to use the experimental data to estimate the parameters of the potential that governs the tip, substrate, and particle interactions.

The results presented here have important implications for high-level programming of nanomanipulation operations. We expect to automate much of the process by exploiting the new knowledge of the underlying phenomena presented here together with our current techniques for compensating for instruments' errors which are embodied in our probe control software. Investigation of phenomena and applications that require positioning of large numbers of particles will become feasible with automated manipulation procedures.

Acknowledgements. This research was supported by the Z.A. Kaprielian Technology Innovation Fund.

References

1. R.F. Service: Science **271**, 920 (1996)
2. A.P. Alivisatos: Science **271**, 933 (1996)
3. D.L. Klein, P.L. McEuen: Appl. Phys. Lett. **68**, 2574 (1996)
4. P.C. Ohara, J.R. Heath, W.M. Gelbart: Angew. Chem. Int. Ed. Engl. **36**, 1077 (1997)
5. R.P. Andres, J.D. Bielefeld, J.I. Henderson, D.B. Janes, V.R. Kolagunta, C.P. Kubiak, W.J. Mahoney, R.G. Osifchin: Science **273**, 1690 (1996)
6. H. Ahmed: J. Vac. Sci. Technol. B **15**, 2101 (1997)
7. T. Junno, K. Deppert, L. Montelius, L. Samuelson: Appl. Phys. Lett. **66**, 3627 (1995)
8. T. Junno, S.B. Carlsson, H. Xu, L. Montelius, L. Samuelson: Appl. Phys. Lett. **72**, 548 (1997)
9. Y. Kim, C.M. Lieber: Science **257**, 375 (1992)
10. D.M. Schaefer, R. Reifenberger, A. Patil, R.P. Andres: Appl. Phys. Lett. **66**, 1012 (1995)
11. C. Baur, B.C. Gazen, B. Koel, T.R. Ramachandran, A.A.G. Requicha, L. Zini: J. Vac. Sci. Technol. B **15**, 1577 (1997)
12. A.A.G. Requicha, C. Baur, A. Bugacov, B.C. Gazen, B. Koel, A. Madhukar, T.R. Ramachandran, R. Resch, P. Will: Proc. IEEE Int'l Conf. on Robotics and Automation, Leuven, Belgium, May 1998
13. J.N. Israelachvili: *Intermolecular and Surface Forces*, 2nd ed (Academic Press, London, San Diego CA, 1991)
14. L. Verlet: Phys. Rev. **159**, 98 (1967)
15. B. Anczykowski, D. Kruger, H. Fuchs: Phys. Rev. B **53**, 15485 (1996)
16. A. Kühle, A.H. Sorensen, J. Bohr: J. Appl. Phys. **81**, 6562 (1997)
17. J.P. Spatz, S. Sheiko, M. Moller, R.G. Winkler, P. Reineker, O. Marti: Nanotechnology **6**, 40 (1995)
18. J. Tamayo, R. Garcia: Langmuir **12**, 4430 (1996)
19. N.A. Burnham, O.P. Behrend, F. Oulevey, G. Gremaud, P.J. Gallo, D. Gourdon, E. Dupas, A.J. Kulik, H.M. Pollock, G.A.D. Briggs: Nanotechnology **8**, 67 (1997)
20. D. Sarid, T.G. Ruskell, R.K. Workman, D. Chen: J. Vac. Sci. Technol. B **14**, 864 (1996)
21. J. de Weger, D. Binks, J. Molenaar, W. van der Water: Phys. Rev. Lett. **76**, 3951 (1996)